*Journal of Sound and Vibration* (2002) **254**(3), 427–446
doi:10.1006/jsvi.2001.4016, available online at http://www.idealibrary.com on IDEAL®

# COUPLED AXIAL–LATERAL–TORSIONAL DYNAMICS OF A ROTOR–BEARING SYSTEM GEARED BY SPUR BEVEL GEARS

M. LI AND H. Y. HU

*Institute of Vibration Engineering Research, Nanjing University of Aeronautics and Astronautics*, 210016 *Nanjing, People's Republic of China*

AND

P. L. JIANG AND L. YU

*Theory of Lubrication and Bearing Institute, Xi'an Jiaotong University*, 710049 *Xi'an, People's Republic of China*

(*Received* 8 *March* 2001, *and in final form* 10 *September* 2001)

The coupled lateral–torsional dynamics of parallel rotor-bearing systems has been intensively investigated. However, little attention has been paid to the analysis of coupled vibrations of angled rotor–bearing systems so that the torsional and the lateral vibrations of those systems are usually analyzed separately. In this paper, the coupled axial–lateral–torsional dynamics of a rotor–bearing system geared by bevel gears is studied. The meshing of two spur bevel gears is analyzed on the basis of a pair of virtual cylindrical gears, and thereafter the constraint condition describing the relationship between the generalized displacements of bevel gears is derived under some assumptions. The coupled dynamic model is established by using Lagrange's equation under this constraint condition. The numerical results of a number of case studies show that the critical speeds of the coupled model are different from those of the uncoupled model both in values and modes, and the threshold speed of stability is fairly less than that of the uncoupled model. The effects of system parameters, such as the pitch cone angles, on the coupling behavior are also discussed.
© 2002 Elsevier Science Ltd. All rights reserved.

## 1. INTRODUCTION

The past two decades have witnessed an intensive study of the coupled lateral–torsional vibrations of parallel geared rotor systems, see, for example in references [1–5]. In geared rotor systems, the lateral displacements of rotors may result in the variation in both torsional angles and geometric parameters of meshing gears. The lateral translations of gear centers may move the common interior tangent to the base circles, and give rise to a variation in the direction of load. Thus, there is an inherent relationship between the dynamic loads and the generalized displacements. It is the primary source of the self-excited vibration in geared rotor systems. The coupling of lateral and torsional vibrations thereby have to be considered.

Almost all the current investigations are limited to the vibrations of such rotating machinery as compressors, where the rotors are parallel to each other and the gears are spur or helical ones. Bevel gears are widely used in various transmission systems of helicopters, ground vehicles, ships and so on because of their capability of transmitting the motion

0022-460X/02/$35.00 © 2002 Elsevier Science Ltd. All rights reserved.

between the two rotors perpendicular to each other. Their dynamics, hence, has begun to receive attention recently. For instance, Hirogaki *et al.* modelled the rotational motion of bevel gears by means of virtual cylindrical gears in reference [6], where the axial, lateral and torsional vibrations were assumed to be decoupled. Li *et al.* computed the critical speeds, the unbalance response and initial bending responses of a miniature engine by using the transfer matrix method in reference [7]. In their study, the relationship between the generalized displacements of the two bevel gears was not taken into consideration. Donley *et al.* in reference [8] developed an approximate dynamic model for hypoid gears by using the finite element method. Lim and Cheng proposed a coupled rotational–translational vibratory model of hypoid geared rotor system to analyze the dynamic effect of pinion offset in reference [9]. To the authors' knowledge, however, no study has been made on the coupled axial–lateral–torsional vibrations in perpendicular geared rotor systems.

Besides the same characteristics as the parallel geared rotor systems, the dynamics of this kind of rotor systems has its own particularity. For example, in a bevel geared rotor system, the axial displacement of one rotor may give rise to the lateral displacement and torsional angle of the other rotor through bevel gears. Namely, the axial, lateral and torsional vibrations of the system may couple with each other. The present paper, therefore, is mainly concerned with the coupling among the axial, torsional and lateral vibrations due to the bevel gear transmission.

## 2. KINETIC CONSTRAINT FOR A PAIR OF SPUR BEVEL GEARS

The tooth surface of a pair of spur bevel gears is the envelope of a family of spherical involute curves. Figure 1 shows a pair of bevel gears, whose transmission can be simplified as a pair of virtual cylindrical gears shown in Figure 2. In this study, the following assumptions upon the system of concern will be used hereinafter:

(1) All the gears or disks are rigid, while the rotors (or shafts) are elastic.
(2) Errors in tooth location and profile are so small that a meshing tooth is in line contact with its mate.
(3) All the generalized displacements are very small, and therefore it is reasonable to use the small perturbation in analysis.

Figure 3 shows a pair of spur bevel gears arranged perpendicularly. This pair can be simplified as a pair of virtual cylindrical gears in the co-ordinate frames $ox_{ei}y_{ei}z_{ei}$, $i = 1, 2$, which are fixed on rotors 1 and 2 respectively. As done in reference [1], the relationship between the lateral translations $x_{e1}$, $y_{e1}$, $x_{e2}$ and $y_{e2}$ of two virtual cylindrical gear centers

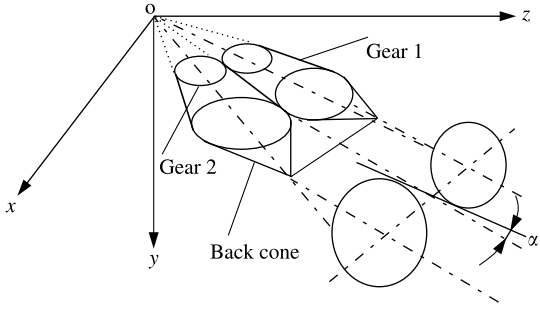


Figure 1. Schematic diagram of a bevel gear pair.

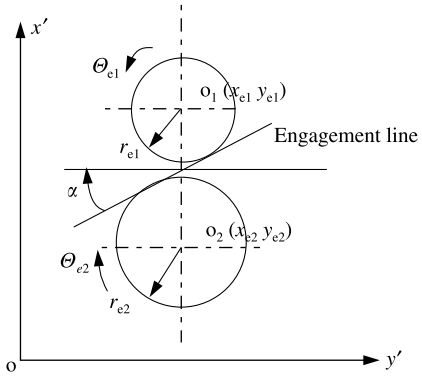


Figure 2. Virtual cylindrical gears.

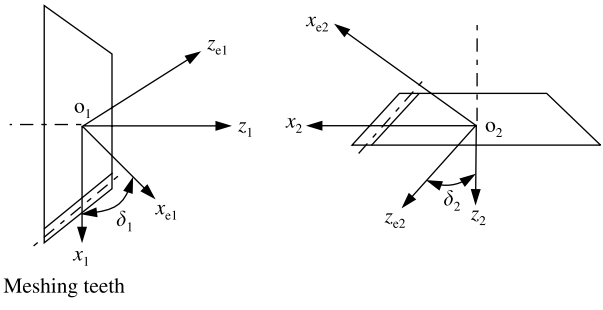


Figure 3. A pair of spur bevel gears.

and the torsional angles $\Theta_{e1}$ and $\Theta_{e2}$ can be simplified to

$$x_{e1}\sin\alpha + y_{e1}\cos\alpha + r_{e1}\Theta_{e1} = x_{e2}\sin\alpha + y_{e2}\cos\alpha + r_{e2}\Theta_{e2}, \tag{1}$$

where $\alpha$ is the pressure angle of gear, $r_{e1}$ and $r_{e2}$ are the radii of base circles of the two virtual cylindrical gears.

As shown in Figure 3, the motion described in the co-ordinate frame $ox_{ei}y_{ei}z_{ei}$ can be determined from

$$\begin{Bmatrix} x_{ei} \\ y_{ei} \\ z_{ei} \end{Bmatrix} = \begin{bmatrix} \cos\delta_i & 0 & \sin\delta_i \\ 0 & 1 & 0 \\ -\sin\delta_i & 0 & \cos\delta_i \end{bmatrix} \begin{Bmatrix} x_i \\ y_i \\ z_i \end{Bmatrix}, \tag{2}$$

where $\delta_i = \delta_1, -\delta_2$, $i = 1, 2$ are the pitch cone angles.

For the virtual cylindrical gears and the bevel gears, the following kinetic relation holds true:

$$r_{ei}\Theta_{ei} = r_{bi}\Theta_i, \tag{3}$$

where $r_{bi}$, $i = 1, 2$ are the radii of base circles of bevel gears. Substituting equations (2) and (3) into equation (1) yields

$$\begin{aligned} &x_1\sin\alpha\cos\delta_1 + y_1\cos\alpha + z_1\sin\alpha\sin\delta_1 + \Theta_1 r_{b1} \\ &\quad = x_2\sin\alpha\cos\delta_2 + y_2\cos\alpha - z_2\sin\alpha\sin\delta_2 + \Theta_2 r_{b2}. \end{aligned} \tag{4}$$

Now, let each torsional angle be composed of two parts as

$$\Theta_i = \Omega_i + \theta_i, \quad i = 1, 2, \tag{5}$$

where $\Omega_i$, $i = 1, 2$ represent the rotating angles of two rotors and yield the transmission relationship of bevel gears

$$\Omega_1 r_{b1} = \Omega_2 r_{b2}. \tag{6}$$

Equation (6) is frequently used in the analysis of torsional vibration of geared rotor systems. Substituting equations (5) and (6) into equation (4) gives the governing equation of small perturbations of motion

$$a_1 x_1 + b_1 y_1 + c_1 z_1 + d_1 \theta_1 = a_2 x_2 + b_2 y_2 + c_2 z_2 + d_2 \theta_2, \tag{7}$$

where the parameters $a_i$, $b_i$, $c_i$, $d_i$, $i = 1, 2$ are only related to the geometry of the teeth profiles as

$$\begin{aligned} a_1 &= \sin\alpha\cos\delta_1, & a_2 &= \sin\alpha\cos\delta_2, \\ b_1 &= \cos\alpha, & b_2 &= \cos\alpha, \\ c_1 &= \sin\alpha\sin\delta_1, & c_2 &= -\sin\alpha\sin\delta_2 \\ d_1 &= r_{b1}, & d_2 &= r_{b2}. \end{aligned} \tag{8}$$

Equation (7) is a kinetic constraint condition of two meshing bevel gears in the system. It indicates a coupling among the axial, lateral and torsional degrees of freedom.

## 3. DYNAMIC MODEL OF A ROTOR SYSTEM GEARED BY BEVEL GEARS

Figure 4 shows a typical bearing–rotor system geared by a pair of spur bevel gears. The system consists of two homogeneous elastic rotors, each of which carries a rigid disk and a straight bevel gear. The rotors are supported on four journal bearings and a thrust bearing. The system can be discretized into $n$ elements on the basis of lumped parameter model. The co-ordinate frames $o_i x_i y_i z_i$, $i = 1, 2$ are used to refer to rotors 1 and 2, respectively, where the planes $x_i z_i$, $i = 1, 2$ are horizontal.

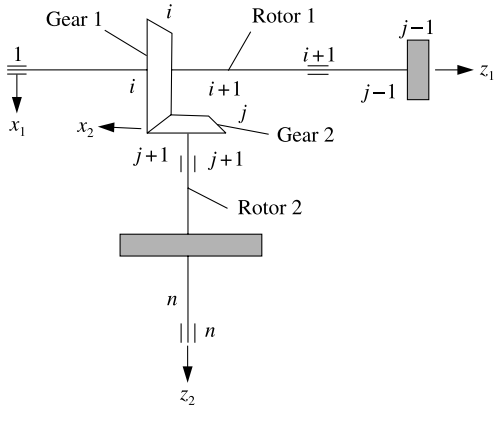


Figure 4. A typical bevel gear–rotor–bearing system.

### 3.1. KINETIC ENERGY

The total kinetic energy of a system is the summation of the translational and rotational kinetic energies of rigid disks, gears and rotors as

$$T = \sum_{i}^{n} \tfrac{1}{2} m_i \mathbf{V}_{ic} \cdot \mathbf{V}_{ic} + \tfrac{1}{2} \mathbf{G}_i \cdot \boldsymbol{\omega}_i. \tag{9}$$

If the terms of higher order are neglected, the kinetic energy can be approximated as

$$T \approx \sum_{i}^{n} [\tfrac{1}{2} m_i (\dot{x}_i^2 + \dot{y}_i^2 + \dot{z}_i^2) + \tfrac{1}{2} J_i^z (\Omega_i + \dot{\theta}_i)^2 + \tfrac{1}{2} J_i^d (\dot{\varphi}_i^2 + \dot{\psi}_i^2) - J_i^z \Omega \varphi_i \dot{\psi}_i], \tag{10}$$

where $m_i$ $(i = 1, 2, \ldots, n)$ is the total lumped mass of the $i$th element, $J_i^j$ $(i = 1, 2, \ldots, n;$ $j = d, z)$ the diametrical and polar moments of inertia, $x_i$, $y_i$, $z_i$, $\varphi_i$, $\psi_i$ and $\theta_i$ the three translational displacements of the mass center, two tilting angles, and torsional angle of the $i$th lumped mass respectively.

### 3.2. POTENTIAL ENERGY

Figure 5 shows the deformation of the $i$th element of rotor, where $S_{i-1}$, $M_{i-1}$, $Q_{i-1}$, $N_{i-1}$, $S_i$, $M_i$, $Q_i$, $N_i$ are the forces and moments acting on the $(i-1)$th and $i$th elements respectively. The potential energy of the system results from the lateral, torsional and axial deformations, i.e.,

$$U = U_t + U_l + U_a. \tag{11}$$

From the equilibrium equation of the $i$th element, one can obtain the transfer equation in $x$ direction as

$$\begin{Bmatrix} x \\ \varphi \\ M \\ S \end{Bmatrix}_i = \begin{bmatrix} 1 & l & \dfrac{l^2}{2EI} & \dfrac{-l^3}{6EI} \\ 0 & 1 & \dfrac{l}{EI} & \dfrac{-l^2}{2EI} \\ 0 & 0 & 1 & -l \\ 0 & 0 & 0 & 1 \end{bmatrix}_j \begin{Bmatrix} x \\ \varphi \\ M \\ S \end{Bmatrix}_{i-i}, \tag{12}$$

where $E$ is the Young's modulus, $I$ the second moment of inertia of the shaft section, $l$ the length of the shaft section. Then, the energy of bending of the $i$th element in direction $x$ can

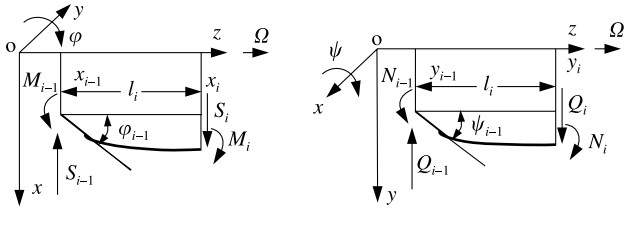


Figure 5. The $i$th element of rotor.

be expressed as

$$\begin{aligned} U_{xi} &= \tfrac{1}{2}(-S_{i-1}x_{i-1} - M_{i-1}\varphi_{i-1} + S_i x_i + M_i \varphi_i) \\ &= \frac{1}{2}\left(\frac{12EI}{l^3}\right)_i (x_i - x_{i-1})^2 - \left(\frac{6EI}{l^2}\right)_i (x_i - x_{i-1})(\varphi_i + \varphi_{i-1}) \\ &\quad + \frac{1}{2}\left(\frac{4EI}{l}\right)_i (\varphi_i^2 + \varphi_i \varphi_{i-1} + \varphi_{i-1}^2). \end{aligned} \tag{13}$$

The potential energy $U_y$ of bending in direction $y$ can be written out in a similar manner. Thus, one has

$$U_l = \sum_i^n (U_{xi} + U_{yi}). \tag{14}$$

The potential energy $U_t$ corresponding to torsional deformation reads as

$$U_t = \sum_i^n \frac{1}{2}\left(\frac{GI_p}{l}\right)_i (\theta_i - \theta_{i-1})^2, \tag{15}$$

where $G$ is the shear modulus, $I_p$ the polar second moment of inertia of the shaft section. Finally, the potential energy $U_a$ corresponding to the axial deformation is

$$U_a = \sum_i^n \frac{1}{2}\left(\frac{EA}{l}\right)_i (z_i - z_{i-1}), \tag{16}$$

where $A$ is the cross-sectional area of shaft.

Substituting equations (13)–(16) into equation (11) yields

$$\begin{aligned} U = \sum_i^n \Bigg[ & \frac{1}{2}\left(\frac{12EI}{l^3}\right)_i (x_i - x_{i-1})^2 - \left(\frac{6EI}{l^2}\right)_i (x_i - x_{i-1})(\varphi_i + \varphi_{i-1}) \\ & + \frac{1}{2}\left(\frac{4EI}{l}\right)_i (\varphi_i^2 + \varphi_i \varphi_{i-1} + \varphi_{i-1}^2) + \frac{1}{2}\left(\frac{12EI}{l^3}\right)_i (y_i - y_{i-1})^2 \\ & - \left(\frac{6EI}{l^2}\right)_i (y_i - y_{i-1})(\psi_i + \psi_{i-1}) + \frac{1}{2}\left(\frac{4EI}{l}\right)_i (\psi_i^2 + \psi_i \psi_{i-1} + \psi_{i-1}^2) \\ & + \frac{1}{2}\left(\frac{GI_p}{l}\right)_i (\theta_i - \theta_{i-1})^2 + \frac{1}{2}\left(\frac{EI}{l}\right)_i (z_i - z_{i-1})^2 \Bigg]. \end{aligned} \tag{17}$$

In the above expressions, the mesh stiffness is not taken into account since it is much higher than the stiffness of shafts in large geared systems.

### 3.3. EQUATIONS OF MOTION

For the geared system shown in Figure 4, equation (7) can be written as

$$\theta_j = [d_t \theta_i + (a_1 x_i + b_1 y_i + c_1 z_i) - (a_2 x_j + b_2 y_j + c_2 z_j)]/d_2. \tag{18}$$

Substituting equation (18) into equations (10) and (17) to eliminate the torsional angle $\theta_j$, and employing Lagrange's equations, one obtains

$$\frac{\mathrm{d}}{\mathrm{d}t}\left(\frac{\partial T}{\partial \dot{q}}\right) - \frac{\partial T}{\partial q} + \frac{\partial U}{\partial q} = Q, \tag{19}$$

where $q = \{\ldots, x_i, y_i, z_i, \varphi_i, \psi_i, \theta_i, \ldots\}^{\mathrm{T}}$ represents the generalized co-ordinates. Each station (or node) in Figure 4 has six degrees of freedom, except that the station on Gear 2 has five. Therefore, the system in Figure 4 has totally $(6n - 1)$ degrees of freedom.

Neglecting the terms of higher order, the dynamic equations on each station can be obtained, where the dynamic equations on Gears 1 and 2 are shown in Appendix A, and those on the other stations are ignored. In fact, these equations can be derived from the finite element method except the ones on two gear stations.

After assembling them, the system equations of motion becomes

$$\mathbf{M}\ddot{\mathbf{q}} + \mathbf{G}\dot{\mathbf{q}} + \mathbf{K}\mathbf{q} = \mathbf{Q}, \tag{20}$$

where the system mass and stiffness matrices **M**, **K** still remain symmetrical in spite of the fact that the equations on Gears 1 and 2 seem to lose their form, and the gyroscopic matrix **G** is skew-symmetrical.

In the case of small vibration, the dynamic forces of a hydrodynamic journal bearing can be expressed in terms of the coefficients of stiffness and damping. The strain energy and the dissipation function of a hydrodynamic journal bearing can be written as

$$\begin{bmatrix} c_{xx} & c_{xy} \\ c_{yx} & c_{yy} \end{bmatrix} \begin{Bmatrix} \dot{x} \\ \dot{y} \end{Bmatrix} + \begin{bmatrix} k_{xx} & k_{xy} \\ k_{yx} & k_{yy} \end{bmatrix} \begin{Bmatrix} x \\ y \end{Bmatrix} = \begin{Bmatrix} \Delta F_x \\ \Delta F_y \end{Bmatrix}, \tag{21}$$

where $k_{xx}$, $k_{xy}$, $k_{yx}$, $k_{yy}$, $c_{xx}$, $c_{xy}$, $c_{yx}$ and $c_{yy}$ are the coefficients of stiffness and damping of the hydrodynamic bearing, which depend on rotational speed and static load on journal bearing. In general, the static bearing loads are related to the transmitted power and system weight. In order to simplify the problem, in the following numerical analysis the load on each bearing is supposed to only depend on the weights of the system, which includes two disks, gears and rotors. Thus, the dynamic equation of the system can be recast as

$$\mathbf{M}\ddot{\mathbf{q}} + (\mathbf{G} + \mathbf{C})\dot{\mathbf{q}} + \mathbf{K}\mathbf{q} = \mathbf{Q}. \tag{22}$$

In general, vector **Q** is composed of external excitations such as the unbalanced force and excitation torque. In matrices **M** and **K**, there exist some entries that couple a part of components in $(\ddot{x}_i, \ddot{y}_i, \ddot{z}_i, \ddot{\theta}_i, \ddot{x}_j, \ddot{y}_j, \ddot{z}_j)$ and $(x_i, y_i, z_i, \theta_i, x_j, y_j, z_j)$ respectively. These entries are related to $a_i$, $b_i$, $c_i$, $d_i$, $i = 1, 2$, $J_j$ and $(GI_p/l)_{j+1}$. That is, the coupled terms are only determined by the geometric parameters of bevel gears and the rotor system. Consequently, the lateral, torsional and axial vibrations couple mutually.

## 4. NUMERICAL RESULTS

In this section, a numerical example is given in order to examine the critical speeds, the threshold speed of stability, and the unbalance responses of the rotor–bearing system geared by bevel gears as shown in Figure 6. In this system, each rotor is discretized into four nodes (node no. 1–4 as rotor 1 and 5–8 as rotor 2), or three beam elements.

In the system shown in Figure 6, each rotor is laterally supported by two journal bearings. There are two identical 360° cylindrical bearings at nodes 1 and 3, and two 5-pad

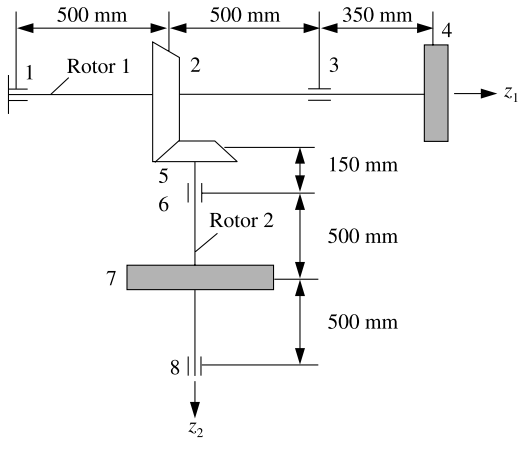


Figure 6. A bearing–rotor system geared by bevel gears.

tilting-pad bearings at nodes 6 and 8 respectively. A rigid axial support is located at node 1 to constrain the axial rigid motion. The parameters of the four journal bearings were taken as follows. The diameter $D_0$ was 100 mm, the ratio $L/D_0$ of length to diameter 0·5, the ratio $\psi$ of clearance 0·002, the dynamic viscosity $\mu$ of oil 0·0221 N s/m$^2$. The eight coefficients of stiffness and damping of bearings were computed under the assumption of short-bearings. The diameter of two rotors was chosen at $d = 100$ mm. The equivalent masses and moments of inertia of gears and disks were set as $m_2 = m_7 = 600$ kg, $m_4 = 300$ kg, $m_5 = 40$ kg, $J_2^l = J_7^l = 15$ kg m$^2$, $J_2^z = J_7^z = 25$ kg m$^2$, $J_4^l = 12$ kg m$^2$, $J_4^z = 20$ kg m$^2$, $J_5^l = 0{\cdot}05$ kg m$^2$, $J_5^z = 0{\cdot}072$ kg m$^2$. The geometric parameters of the bevel gears were taken as $\alpha = 20^\circ$, $\delta_1 = 70^\circ$, $\delta_2 = 20^\circ$, $r_{b1} = 300$ mm, $r_{b2} = 100$ mm. The material constants of the rotors were assumed to be $E = 206$ GN/m$^2$ and $G = 78$ GN/m$^2$.

### 4.1. CRITICAL SPEEDS AND MODES

When the vector $\mathbf{Q}$ of generalized external force vanishes, equation (22) governs the free vibration of the system. The corresponding eigenvalue problem can be solved by using the generalized inverse iteration method in reference [10].

As a part of the design procedure of a geared rotor system, it is usual to compute the critical torsional speeds of the transmission train, and then the critical lateral speed of each rotor as well [1]. This is called the computation based on the uncoupled model for short. In the torsional analysis of the critical speeds or natural frequencies, the bevel gear branched system shown in Figure 6 can readily be seen as an idealized one shown in Figure 7, where $J_1 = J_7^z r_{b1}^2/r_{b2}^2$, $J_2 = J_5^z r_{b1}^2/r_{b2}^2 + J_2^z$, $J_3 = J_4^z$, $k_1 = (GI_p/L_1)\, r_{b1}^2/r_{b2}^2$, $k_2 = GI_p/L_2$, $L_1 = 650$ mm, $L_2 = 850$ mm. The natural frequencies are $\omega_{t1} = 213{\cdot}2$ rad/s, $\omega_{t2} = 705{\cdot}7$ rad/s.

The critical speed of the coupled axial–lateral–torsional model is defined as the speed of the rotor system when it is equal to the imaginary part of one of the eigenvalues of the system. For simplicity, only the critical speeds and corresponding modes of the rigidly supported system were computed. Table 1 gives the lowest critical speeds of rotor 1, rotor 2 and the coupled model respectively. The corresponding mode shapes of the coupled model are shown in Figure 8, where the horizontal axis represents the node number of the rotors (1–4 as rotor 1 and 5–8 as rotor 2), and the vertical axis the dimensionless generalized displacements.

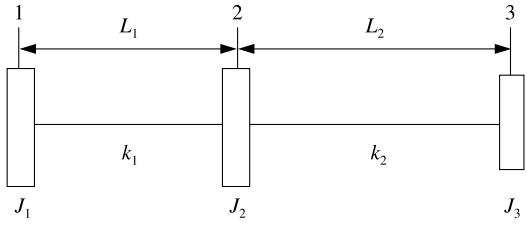


Figure 7. The torsional idealized model of the geared system.

TABLE 1

*Critical speeds of the rigidly supported rotor system (r.p.m.)*

| Mode | 1st | 2nd | 3rd | 4th | 5th | 6th | 7th | 11th |
|---|---|---|---|---|---|---|---|---|
| Rotor 1 | 1476 | 2117 | 3491 | — | — | — | — | — |
| Rotor 2 | 2695 | 2698 | 5240 | — | — | — | — | — |
| Coupled model | 1399 | 1743 | 2265 | 2694 | 2706 | 3347 | 3501 | 16086 |
| Coupled model† | 1399 | 1745 | 2267 | 2695 | 2704 | 3334 | 3501 | 16078 |

† In this case, $\delta_1 = 60^\circ$ and $\delta_2 = 30^\circ$.

From Table 1 and Figure 8, it is obvious that the lateral components of the first, second, third and sixth modes, corresponding to the critical speed at 1399, 1743, 2265 and 3347 r.p.m. of the coupled model mainly stem from the first three modes of rotor 1, while the fourth and fifth modes, corresponding to 2694 and 2706 r.p.m. from the first two critical speeds of rotor 2. In these modes, the axial component is negligible, and only the coupling between lateral and torsional vibrations is remarkable. The mode of the seventh critical speed is almost composed of perfectly lateral components of the two rotors. This implies that the coupling among the three kinds of vibrations is very weak. The perfectly torsional frequencies, computed from the perfectly torsional model as shown in Figure 7, are insignificant in the coupled model because they vary greatly both in modes and values. Therefore, when calculating the critical speeds or the natural frequencies in the rotor system geared by bevel gears, the perfectly lateral or perfectly torsional model may lose some very important coupled modes. In the above modes, the components of the axial displacement are very small because the axial stiffness is much larger than the lateral and torsional ones of the system. The 11th mode shown in Figure 8(h) vibrates mainly in the axial direction.

Table 1 also gives the critical speeds when $\delta_1 = 60^\circ$ and $\delta_2 = 30^\circ$. The results indicate that the critical speeds almost do not vary with the pitch cone angles.

### 4.2. SYSTEM STABILITY

In geared rotor–bearing system, the eigenvalues as well as eigenvectors in most cases occur in conjugate complex pairs. The smallest real part of eigenvalues reflects the stability of a stable system. That is, the ability of the system to resist any external disturbance. The threshold speed of stability is defined as the lowest speed when the real part of one of the eigenvalues is equal to zero.

Table 2 gives the threshold speeds of stability computed from the individual rotor–bearing model and the coupled axial–lateral–torsional model of the rotor–bearing

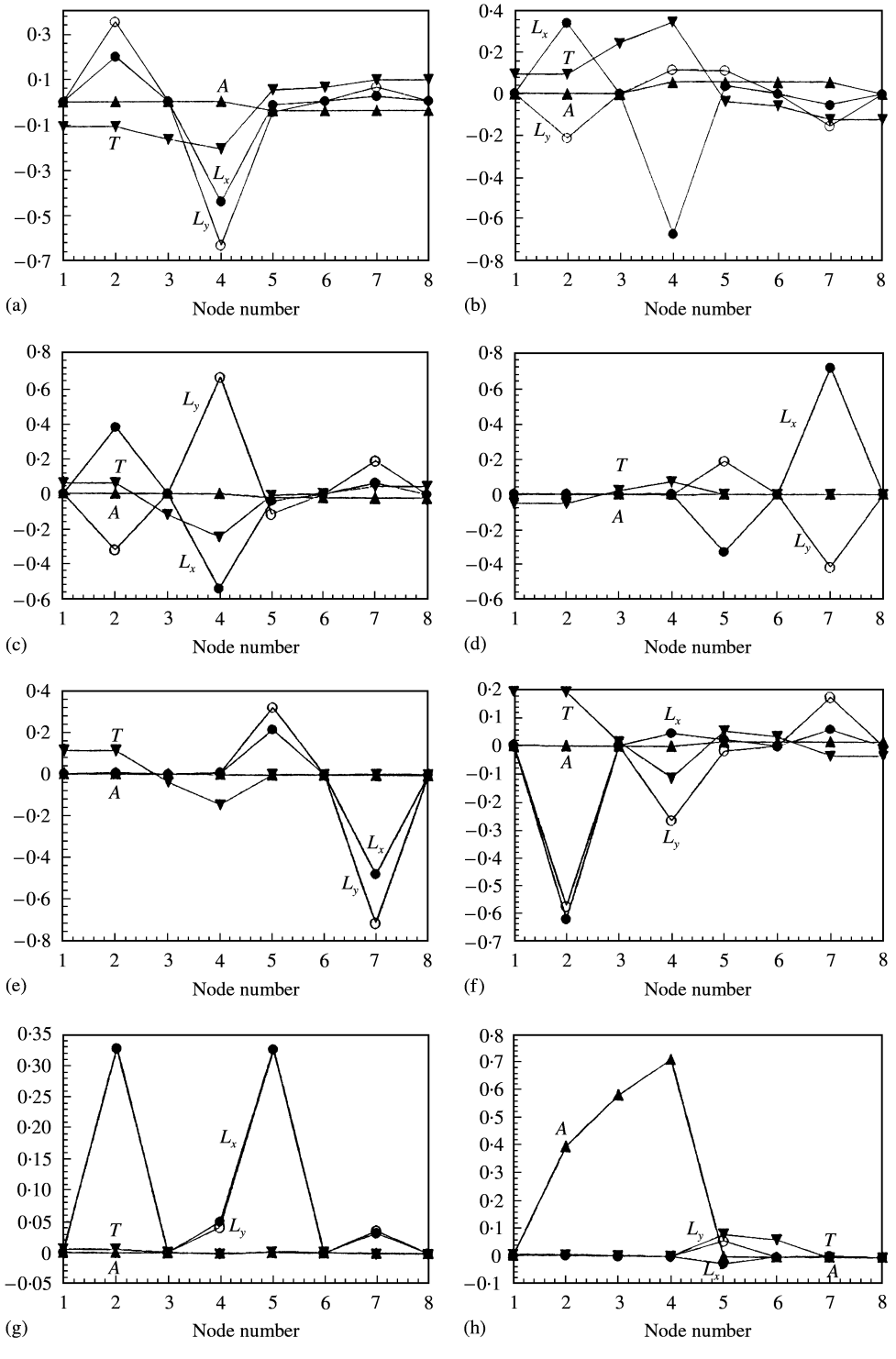


Figure 8. Mode shapes and critical speeds of the rigidly supported system. (a) 1399 r.p.m.; (b) 1743 r.p.m.; (c) 2265 r.p.m.; (d) 2694 r.p.m.; (e) 2706 r.p.m.; (f) 3347 r.p.m.; (g) 3501 r.p.m.; (h) 16086 r.p.m. —●—, $L_x$ lateral displacement in $x$ direction; —○—, $L_y$ lateral displacement in $y$ direction; —▲—, $A$ axial direction; —▼—, $T$ torsional direction.

TABLE 2

*Threshold speed of stability of the system supported by oil film bearings (r.p.m.)*

| | Rotor 1 | Rotor 2 | Coupled model | Coupled model† |
|---|---|---|---|---|
| Speed | 4050 | ≫20000 | 3041 | 3033 |

†In this case, $\delta_1 = 60^\circ$ and $\delta_2 = 30^\circ$.

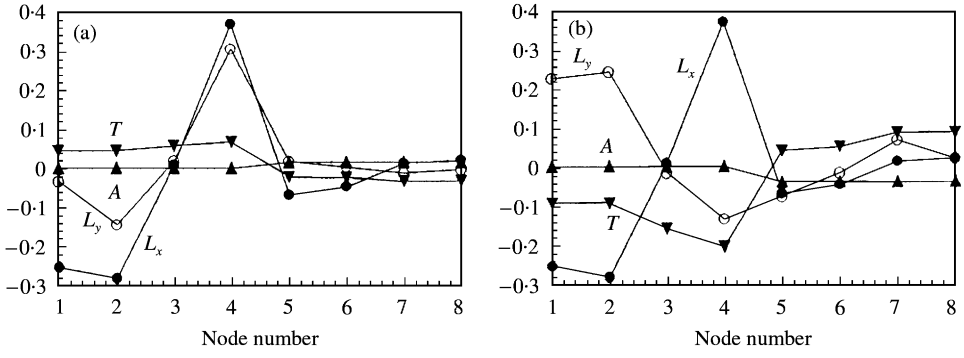


Figure 9. The first two mode shapes at stability threshold speed when the rotors are supported by hydrodynamic bearings: (a) mode 1; (b) mode 2. —●—, $L_x$ lateral displacement in $x$ direction; —○—, $L_y$ lateral displacement in $y$ direction; —▲—, $A$ axial direction; —▼—, $T$ torsional direction.

system geared by bevel gears respectively. Figure 9 shows the first two mode shapes of the system at the threshold speed of stability based on the coupled model, where mode 1 is stable, and mode 2 is unstable. In the figure, the vertical axis represents the modulus of dimensionless generalized displacements, and the horizontal axis still represents the node number of the rotors (1–4 as rotor 1 and 5–8 as rotor 2). From Table 2, the threshold speed of rotor 2 is very high because it is supported by tilting-pad bearings. Therefore, the stability of the system mainly depends on that of rotor 1. When the coupling is considered, the threshold speed of stability is decreased by 24·9% and becomes 3041 r.p.m. At this speed, the lateral components are predominant in the corresponding mode (mode 2), which is followed by the torsional one, while the axial one is the smallest. When the rotating speed of rotor 1 is 2800 r.p.m. (meanwhile rotor 2 is 8400 r.p.m.), the stability of system deteriorates. This phenomenon has been found in parallel geared rotor system; Schwibinger and Nordmann [4] explained that the stability behavior of the coupled torsional–lateral vibration of their rotor–bearing system was affected by the energy exchange between the torsional and the lateral system. Because torsional and lateral displacements are coupled in gear stage, torsional oscillations of the geared rotor train are also excited. In bevel geared rotor system, because the geared rotor system is coupled in axial, torsional and lateral directions, this results in the fact that the mass, damping, and stiffness matrices of the whole system are changed, which make the eigenvalues and eigenvectors of the system varied. That is, the instability behavior as well as nature characteristics of the system are influenced. Then why is the threshold speed of stability decreased in bevel geared rotor–bearing system, not increased? Intuitively, this result results in the fact that the system damping mainly provided by the journal bearings only takes the effect in the lateral vibrations. The coupling among the axial, lateral and torsional vibrations enables the axial and torsional vibrations to share this damping with the lateral vibrations. In other words, the energy exchange

among the axial, the lateral and the torsional vibrations occurs at the gear mesh. This leads to the deterioration of the system stability.

Table 2 indicates that the threshold speed of stability of the coupled model is affected by the pitch cone angles $\delta_1$ and $\delta_2$. It is obvious that the speed changes only a little.

### 4.3. UNBALANCE RESPONSES

Two case studies were made for different offsets of unbalance. In the first case, the offset of unbalance was supposed to be 0·01 mm at the gear on rotor 1. Figure 10 shows the variations of the unbalance responses at each node versus rotating speed. The results indicate that the unbalance on rotor 1 can evoke the responses of rotor 2 because of the coupling, and the frequencies of the peak responses of rotor 2 correspond to those of rotor 1. Compared with the uncoupled model, the coupling model increases the lateral amplitude of unbalance response at bearing 1 by 22% at the rotating speed of 2800 r.p.m. for rotor 1, but decreases the amplitude at bearing 2 by 4%.

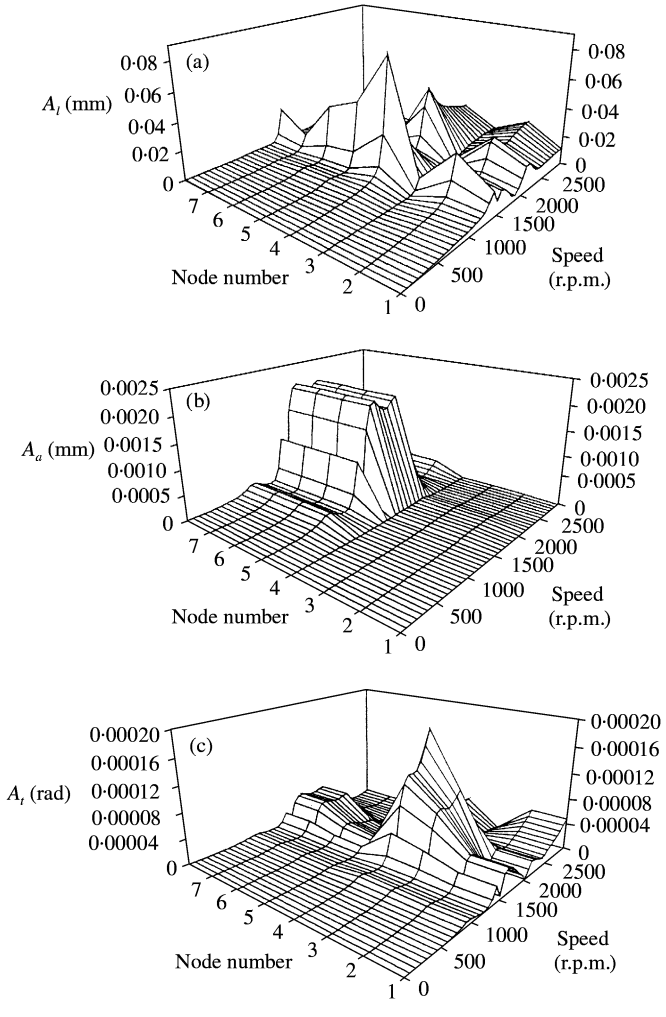


Figure 10. Unbalance responses in three directions: (a) lateral; (b) axial; (c) torsional.

In the second case, the offset of unbalance was supposed to be 0·01 mm at the disk on rotor 2. Figure 11 shows the variations of the unbalance responses at each node with respect to the rotating speed. The results also indicate that the unbalance responses are evoked not only in the lateral direction, but also in the axial and torsional directions. In Figures 10(b) and 11(b), the responses at nodes 1–4 are very small because the freedom in the axial direction at node 1 is constrained. Moreover, in the case of $\delta_1 = 60^\circ$ and $\delta_2 = 30^\circ$, the unbalance responses will be modified, but the change is not large. If the rotor is subject to an external moment (or force) in the torsional (or axial) direction, the responses in three directions will be observed because of the coupling.

## 5. CONCLUSIONS

In this paper, a kinetic constraint equation for the generalized displacements of a pair of bevel gears is formulated under a few assumptions. Using this constraint equation and Lagrange's approach, the dynamic equation of the coupled axial–lateral–torsional

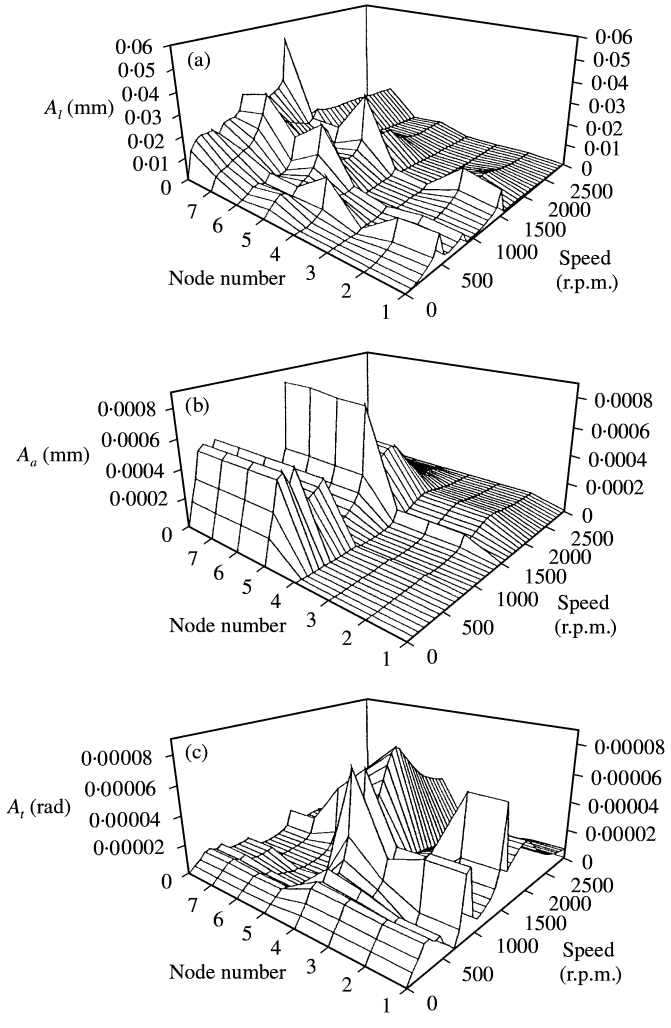


Figure 11. Unbalance responses in three directions: (a) lateral; (b) axial; (c) torsional.

vibrations of rotor system geared by a pair of bevel gears is established. The results show that the axial vibration, lateral vibration, and torsional vibration are coupled mutually and should not be analyzed separately. In addition, an example is given for analyzing the dynamic characteristics such as the critical speeds, the threshold speed of stability and the unbalance response of the geared rotor system. The numerical results indicate that the coupling between the lateral and torsional vibrations is much more significant in the system than other couplings. Some case studies are also presented for the variation of pitch cone angles. These results are beneficial in understanding the coupled axial–lateral–torsional vibrations for the rotor system geared by bevel gears.

## REFERENCES


1. J. W. LUND 1978 *Transactions of American Society of Mechanical Engineers, Journal of Mechanical Design* **100**, 535–539. Critical speed, stability and response of a geared train of rotors.
2. T. IWATSUBO, S. ARII and P. KAWAI 1984 *Proceedings Imech E: C* **265**, 59–66. The coupled lateral torsional vibration of a geared rotor system.
3. H. IIDA, A. TAMURA, K. KIKUCH, *et al.* 1980 *Bulletin of JSME* **23**, 2111–2117. Coupled torsional–flexural vibration of a shaft in a geared system of rotors.
4. P. SCHWIBINGER and R. NORDMANN 1988 *Transactions of American Society of Mechanical Engineers, Journal of Engineering for Gas Turbines and Power* **110**, 563–571. The influence of torsional–lateral coupling on stability behavior of geared rotor system.
5. T. ZUETBES 1989 *Rotating Machinery Dynamics* **18**, 217–224. Stability behavior of geared rotor systems regarding torsional lateral coupling.
6. T. HIROGAKI, E. AOYAMA, Y. UENISI, *et al.* 1996 *Transactions of Japan Society of Precision Engineering Part C* **62**, 1998–2004. Study on dynamic behavior of the Oerlikon-type spiral bevel gears (rotational vibration of gears under running conditions).
7. Z. G. LI, Y. YANG, P. Z. REN, *et al.* 1998 *Tuijin Jishu Journal of Propulsion Technology* **19**, 40–44. Calculation and analysis of vibration characteristics for a miniature engine.
8. M. G. DONLEY, T. C. LIM and G. C. STEYER 1992 *Journal of Passenger Cars* **101**, 77–87. Dynamic analysis of automotive gearing systems.
9. T. C. LIM and Y. CHENG 1999 *Transactions of American Society of Mechanical Engineers, Journal of Mechanical Design* **121**, 535–539. A theoretical study of the effect of pinion offset on the dynamics of hypoid geared rotor system.
10. T. S. ZHENG, W. M. LIU and Z. B. CAI 1989 *Computers and Structures* **33**, 1139–1143. A generalized inverse iteration method for solution of quadratic eigenvalues problems in structural dynamic analysis.


## APPENDIX A: DYNAMIC EQUATIONS ON GEARS

Dynamic equations on Gear 1 (the $i$th station in Figure 4) are as follows:

$$\begin{bmatrix}
m_i + \frac{a_1}{d_2^2} J_j^z & \frac{a_1 b_1}{d_2^2} J_j^z & \frac{a_1 c_1}{d_2^2} J_j^z & 0 & 0 & \frac{a_1 d_1}{d_2^2} J_j^z \\
\frac{a_1 b_1}{d_2^2} J_j^z & m_i + \frac{b_1^2}{d_2^2} J_j^z & \frac{b_1 c_1}{d_2^2} J_j^z & 0 & 0 & \frac{b_1 d_1}{d_2^2} J_j^z \\
\frac{a_1 c_1}{d_2^2} J_j^z & \frac{b_1 c_1}{d_2^2} J_j^z & m_i + \frac{c_1^2}{d_2^2} J_j^z & 0 & 0 & \frac{c_1 d_1}{d_2^2} J_j^z \\
0 & 0 & 0 & J_i^d & 0 & 0 \\
0 & 0 & 0 & 0 & J_i^d & 0 \\
\frac{a_1 d_1}{d_2^2} J_j^z & \frac{b_1 d_1}{d_2^2} J_j^z & \frac{c_1 d_1}{d_2^2} J_j^z & 0 & 0 & J_i^z + \frac{d_1^2}{d_2^2} J_j^z
\end{bmatrix}
\begin{Bmatrix} \ddot{x}_i \\ \ddot{y}_i \\ \ddot{z}_i \\ \ddot{\varphi}_i \\ \ddot{\psi}_i \\ \ddot{\theta}_i \end{Bmatrix}$$

$$
-\begin{bmatrix}
\frac{a_1a_2}{d_2^2}J_j^z & \frac{a_1b_2}{d_2^2}J_j^z & \frac{a_1c_2}{d_2^2}J_j^z & 0 & 0 & 0\\
\frac{a_2b_1}{d_2^2}J_j^z & \frac{b_1b_2}{d_2^2}J_j^z & \frac{b_1c_2}{d_2^2}J_j^z & 0 & 0 & 0\\
\frac{a_2c_1}{d_2^2}J_j^z & \frac{bc_1}{d_2^2}J_j^z & \frac{c_1c_2}{d_2^2}J_j^z & 0 & 0 & 0\\
0 & 0 & 0 & 0 & 0 & 0\\
0 & 0 & 0 & 0 & 0 & 0\\
\frac{a_2d_1}{d_2^2}J_j^z & \frac{b_2d_1}{d_2^2}J_j^z & \frac{c_2d_1}{d_2^2}J_j^z & 0 & 0 & 0
\end{bmatrix}
\begin{Bmatrix}
\ddot{x}_j\\ \ddot{y}_j\\ \ddot{z}_j\\ \ddot{\varphi}_j\\ \ddot{\psi}_j\\ \ddot{\theta}_j
\end{Bmatrix}
$$

$$
+\begin{bmatrix}
0 & 0 & 0 & 0 & 0 & 0\\
0 & 0 & 0 & 0 & 0 & 0\\
0 & 0 & 0 & 0 & 0 & 0\\
0 & 0 & 0 & 0 & J_j^z\Omega_1 & 0\\
0 & 0 & 0 & -J_i^z\Omega_1 & 0 & 0\\
0 & 0 & 0 & 0 & 0 & 0
\end{bmatrix}
\begin{Bmatrix}
\dot{x}_i\\ \dot{y}_i\\ \dot{z}_i\\ \dot{\varphi}_i\\ \dot{\psi}_i\\ \dot{\theta}_i
\end{Bmatrix}
$$

$$
+\begin{bmatrix}
\frac{12EI}{l^3} & 0 & 0 & -\frac{6EI}{l^2} & 0 & 0\\
0 & \frac{12EI}{l^3} & 0 & 0 & -\frac{6EI}{l^2} & 0\\
0 & 0 & \frac{EA}{l} & 0 & 0 & 0\\
-\frac{6EI}{l^2} & 0 & 0 & \frac{4EI}{l} & 0 & 0\\
0 & -\frac{6EI}{l^2} & 0 & 0 & \frac{4EI}{l} & 0\\
0 & 0 & 0 & 0 & 0 & \frac{GI_p}{l}
\end{bmatrix}_i
\begin{Bmatrix}
x_i\\ y_i\\ z_i\\ \varphi_i\\ \psi_i\\ \theta_i
\end{Bmatrix}
$$

$$
+\begin{bmatrix}
\frac{12EI}{l^3} & 0 & 0 & \frac{6EI}{l^2} & 0 & 0\\
0 & \frac{12EI}{l^3} & 0 & 0 & \frac{6EI}{l^2} & 0\\
0 & 0 & \frac{EA}{l} & 0 & 0 & 0\\
\frac{6EI}{l^2} & 0 & 0 & \frac{4EI}{l} & 0 & 0\\
0 & \frac{6EI}{l^2} & 0 & 0 & \frac{4EI}{l} & 0\\
0 & 0 & 0 & 0 & 0 & \frac{GI_p}{l}
\end{bmatrix}_{i+1}
\begin{Bmatrix}
x_i\\ y_i\\ z_i\\ \varphi_i\\ \psi_i\\ \theta_i
\end{Bmatrix}
$$

$$
-\begin{bmatrix}
\frac{12EI}{l^3} & 0 & 0 & \frac{6EI}{l^2} & 0 & 0 \\
0 & \frac{12EI}{l^3} & 0 & 0 & \frac{6EI}{l^2} & 0 \\
0 & 0 & \frac{EA}{l} & 0 & 0 & 0 \\
-\frac{6EI}{l^2} & 0 & 0 & -\frac{2EI}{l} & 0 & 0 \\
0 & -\frac{6EI}{l^2} & 0 & 0 & -\frac{2EI}{l} & 0 \\
0 & 0 & 0 & 0 & 0 & \frac{GI_p}{l}
\end{bmatrix}_i
\begin{Bmatrix} x_{i-1} \\ y_{i-1} \\ z_{i-1} \\ \varphi_{i-1} \\ \psi_{i-1} \\ \theta_{i-1} \end{Bmatrix}
$$

$$
-\begin{bmatrix}
\frac{12EI}{l^3} & 0 & 0 & -\frac{6EI}{l^2} & 0 & 0 \\
0 & \frac{12EI}{l^3} & 0 & 0 & -\frac{6EI}{l^2} & 0 \\
0 & 0 & \frac{EA}{l} & 0 & 0 & 0 \\
\frac{6EI}{l^2} & 0 & 0 & -\frac{2EI}{l} & 0 & 0 \\
0 & \frac{6EI}{l^2} & 0 & 0 & -\frac{2EI}{l} & 0 \\
0 & 0 & 0 & 0 & 0 & \frac{GI_p}{l}
\end{bmatrix}_{i+1}
\begin{Bmatrix} x_{i+1} \\ y_{i+1} \\ z_{i+1} \\ \varphi_{i+1} \\ \psi_{i+1} \\ \theta_{i+1} \end{Bmatrix}
$$

$$
+\begin{bmatrix}
\frac{a_1^2}{d_2^2}\frac{GI_p}{l} & \frac{a_1b_1}{d_2^2}\frac{GI_p}{l} & \frac{a_1c_1}{d_2^2}\frac{GI_p}{l} & 0 & 0 & \frac{a_1d_1}{d_2^2}\frac{GI_p}{l} \\
\frac{a_1b_1}{d_2^2}\frac{GI_p}{l} & \frac{b_1^2}{d_2^2}\frac{GI_p}{l} & \frac{b_1c_1}{d_2^2}\frac{GI_p}{l} & 0 & 0 & \frac{b_1d_1}{d_2^2}\frac{GI_p}{l} \\
\frac{a_1c_1}{d_2^2}\frac{GI_p}{l} & \frac{b_1c_1}{d_2^2}\frac{GI_p}{l} & \frac{c_1^2}{d_2^2}\frac{GI_p}{l} & 0 & 0 & \frac{c_1d_1}{d_2^2}\frac{GI_p}{l} \\
0 & 0 & 0 & 0 & 0 & 0 \\
0 & 0 & 0 & 0 & 0 & 0 \\
\frac{a_1d_1}{d_2^2}\frac{GI_p}{l} & \frac{b_1d_1}{d_2^2}\frac{GI_p}{l} & \frac{c_1d_1}{d_2^2}\frac{GI_p}{l} & 0 & 0 & \frac{d_1^2}{d_2^2}\frac{GI_p}{l}
\end{bmatrix}_{j+1}
\begin{Bmatrix} x_i \\ y_i \\ z_i \\ \varphi_i \\ \psi_i \\ \theta_i \end{Bmatrix}
$$

$$-\begin{bmatrix} \frac{a_1a_2}{d_2^2}\frac{GI_p}{l} & \frac{a_1b_2}{d_2^2}\frac{GI_p}{l} & \frac{a_1c_2}{d_2^2}\frac{GI_p}{l} & 0 & 0 & \frac{a_1d_2}{d_2^2}\frac{GI_p}{l} \\ \frac{a_2b_1}{d_2^2}\frac{GI_p}{l} & \frac{b_1b_2}{d_2^2}\frac{GI_p}{l} & \frac{b_1c_2}{d_2^2}\frac{GI_p}{l} & 0 & 0 & \frac{b_1d_2}{d_2^2}\frac{GI_p}{l} \\ \frac{a_2c_1}{d_2^2}\frac{GI_p}{l} & \frac{b_2c_1}{d_2^2}\frac{GI_p}{l} & \frac{c_1c_2}{d_2^2}\frac{GI_p}{l} & 0 & 0 & \frac{c_1d_2}{d_2^2}\frac{GI_p}{l} \\ 0 & 0 & 0 & 0 & 0 & 0 \\ 0 & 0 & 0 & 0 & 0 & 0 \\ \frac{a_2d_1}{d_2^2}\frac{GI_p}{l} & \frac{b_2d_1}{d_2^2}\frac{GI_p}{l} & \frac{c_2d_1}{d_2^2}\frac{GI_p}{l} & 0 & 0 & \frac{d_1d_2}{d_2^2}\frac{GI_p}{l} \end{bmatrix}_{j+1} \begin{Bmatrix} x_j \\ y_j \\ z_j \\ \varphi_j \\ \psi_j \\ \theta_j \end{Bmatrix} = 0$$

and the dynamic equations on Gear 2 (the $j$th station in Figure 4) are

$$\begin{bmatrix} m_j + \frac{a_2^2}{d_2^2}J_j^z & \frac{a_2b_2}{d_2^2}J_j^z & \frac{a_2c_2}{d_2^2}J_j^z & 0 & 0 & 0 \\ \frac{a_2b_2}{d_2^2}J_j^z & m_j + \frac{b_2^2}{d_2^2}J_j^z & \frac{b_2c_2}{d_2^2}J_j^z & 0 & 0 & 0 \\ \frac{a_2c_2}{d_2^2}J_j^z & \frac{b_2c_2}{d_2^2}J_j^z & m_j + \frac{c_2^2}{d_2^2}J_j^z & 0 & 0 & 0 \\ 0 & 0 & 0 & J_j^d & 0 & 0 \\ 0 & 0 & 0 & 0 & J_j^d & 0 \\ 0 & 0 & 0 & 0 & 0 & 0 \end{bmatrix} \begin{Bmatrix} \ddot{x}_j \\ \ddot{y}_j \\ \ddot{z}_j \\ \ddot{\varphi}_j \\ \ddot{\psi}_j \\ \ddot{\theta}_j \end{Bmatrix}$$

$$-\begin{bmatrix} \frac{a_1a_2}{d_2^2}J_j^z & \frac{a_2b_1}{d_2^2}J_j^z & \frac{a_2c_1}{d_2^2}J_j^z & 0 & 0 & \frac{a_2d_1}{d_2^2}J_j^z \\ \frac{a_1b_2}{d_2^2}J_j^z & \frac{b_1b_2}{d_2^2}J_j^z & \frac{b_2c_1}{d_2^2}J_j^z & 0 & 0 & \frac{b_2d_1}{d_2^2}J_j^z \\ \frac{a_1c_2}{d_2^2}J_j^z & \frac{b_1c_2}{d_2^2}J_j^z & \frac{c_1c_2}{d_2^2}J_j^z & 0 & 0 & \frac{c_2d_1}{d_2^2}J_j^z \\ 0 & 0 & 0 & 0 & 0 & 0 \\ 0 & 0 & 0 & 0 & 0 & 0 \\ 0 & 0 & 0 & 0 & 0 & 0 \end{bmatrix} \begin{Bmatrix} \ddot{x}_i \\ \ddot{y}_i \\ \ddot{z}_i \\ \ddot{\varphi}_i \\ \ddot{\psi}_i \\ \ddot{\theta}_i \end{Bmatrix}$$

$$+\begin{bmatrix} 0 & 0 & 0 & 0 & 0 & 0 \\ 0 & 0 & 0 & 0 & 0 & 0 \\ 0 & 0 & 0 & 0 & 0 & 0 \\ 0 & 0 & 0 & 0 & J_j^z\Omega_2 & 0 \\ 0 & 0 & 0 & -J_i^z\Omega_2 & 0 & 0 \\ 0 & 0 & 0 & 0 & 0 & 0 \end{bmatrix} \begin{Bmatrix} \dot{x}_j \\ \dot{y}_j \\ \dot{z}_j \\ \dot{\varphi}_j \\ \dot{\psi}_j \\ \dot{\theta}_j \end{Bmatrix}$$

$$+\begin{bmatrix} \frac{12EI}{l^3} & 0 & 0 & \frac{6EI}{l^2} & 0 & 0 \\ 0 & \frac{12EI}{l^3} & 0 & 0 & \frac{6EI}{l^2} & 0 \\ 0 & 0 & \frac{EA}{l} & 0 & 0 & 0 \\ \frac{6EI}{l^2} & 0 & 0 & \frac{4EI}{l} & 0 & 0 \\ 0 & \frac{6EI}{l^2} & 0 & 0 & \frac{4EI}{l} & 0 \\ 0 & 0 & 0 & 0 & 0 & 0 \end{bmatrix}_{j+1} \begin{Bmatrix} x_j \\ y_j \\ z_j \\ \varphi_j \\ \psi_j \\ \theta_j \end{Bmatrix}$$

$$-\begin{bmatrix} \frac{12EI}{l^3} & 0 & 0 & -\frac{6EI}{l^2} & 0 & 0 \\ 0 & \frac{12EI}{l^3} & 0 & 0 & -\frac{6EI}{l^2} & 0 \\ 0 & 0 & \frac{EA}{l} & 0 & 0 & 0 \\ \frac{6EI}{l^2} & 0 & 0 & -\frac{2EI}{l} & 0 & 0 \\ 0 & \frac{6EI}{l^2} & 0 & 0 & -\frac{2EI}{l} & 0 \\ 0 & 0 & 0 & 0 & 0 & \frac{GI_p}{l} \end{bmatrix}_{j+1} \begin{Bmatrix} x_{j+1} \\ y_{j+1} \\ z_{j+1} \\ \varphi_{j+1} \\ \psi_{j+1} \\ \theta_{j+1} \end{Bmatrix}$$

$$+\begin{bmatrix} \frac{a_2^2}{d_2^2}\frac{GI_p}{l} & \frac{a_2b_2}{d_2^2}\frac{GI_p}{l} & \frac{a_2c_2}{d_2^2}\frac{GI_p}{l} & 0 & 0 & \frac{a_2d_2}{d_2^2}\frac{GI_p}{l} \\ \frac{a_2b_2}{d_2^2}\frac{GI_p}{l} & \frac{b_2^2}{d_2^2}\frac{GI_p}{l} & \frac{b_2c_2}{d_2^2}\frac{GI_p}{l} & 0 & 0 & \frac{b_2d_2}{d_2^2}\frac{GI_p}{l} \\ \frac{a_2c_2}{d_2^2}\frac{GI_p}{l} & \frac{b_2c_2}{d_2^2}\frac{GI_p}{l} & \frac{c_2^2}{d_2^2}\frac{GI_p}{l} & 0 & 0 & \frac{c_2d_2}{d_2^2}\frac{GI_p}{l} \\ 0 & 0 & 0 & 0 & 0 & 0 \\ 0 & 0 & 0 & 0 & 0 & 0 \\ 0 & 0 & 0 & 0 & 0 & 0 \end{bmatrix}_{j+1} \begin{Bmatrix} x_j \\ y_j \\ z_j \\ \varphi_j \\ \psi_j \\ \theta_{j+1} \end{Bmatrix}$$

$$-\begin{bmatrix} \frac{a_1a_2}{d_2^2}\frac{GI_p}{l} & \frac{a_2b_1}{d_2^2}\frac{GI_p}{l} & \frac{a_2c_1}{d_2^2}\frac{GI_p}{l} & 0 & 0 & \frac{a_2d_1}{d_2^2}\frac{GI_p}{l} \\ \frac{a_1b_2}{d_2^2}\frac{GI_p}{l} & \frac{b_1b_2}{d_2^2}\frac{GI_p}{l} & \frac{b_2c_1}{d_2^2}\frac{GI_p}{l} & 0 & 0 & \frac{b_2d_1}{d_2^2}\frac{GI_p}{l} \\ \frac{a_1c_2}{d_2^2}\frac{GI_p}{l} & \frac{b_1c_2}{d_2^2}\frac{GI_p}{l} & \frac{c_1c_2}{d_2^2}\frac{GI_p}{l} & 0 & 0 & \frac{c_2d_1}{d_2^2}\frac{GI_p}{l} \\ 0 & 0 & 0 & 0 & 0 & 0 \\ 0 & 0 & 0 & 0 & 0 & 0 \\ 0 & 0 & 0 & 0 & 0 & 0 \end{bmatrix}_{j+1} \begin{Bmatrix} x_i \\ y_i \\ z_i \\ \varphi_i \\ \psi_i \\ \theta_i \end{Bmatrix} = 0.$$

## APPENDIX B: NOMENCLATURE

| | |
|---|---|
| $A$ | amplitude |
| $E$ | Young's modulus |
| $G$ | shear modulus |
| $\mathbf{G}$ | vector of angular momentum |
| $J_1, J_2, J_3$ | equivalent polar inertia moments in Figure 7 |
| $I, I_p$ | second moment and polar second moment of area |
| $L_1, L_2$ | lengths of the equivalent shaft in Figure 7 |
| $S, M, Q, N$ | forces and bending moments acting on the end of shaft section |
| $T$ | kinetic energy |
| $U$ | potential energy |
| $\mathbf{G}$ | gyroscopic matrix |
| $\mathbf{M}, \mathbf{C}, \mathbf{K}$ | matrices of generalized mass, damping and stiffness |
| $\mathbf{Q}$ | vector of generalized force |
| $\mathbf{V}$ | vector of generalized velocity |
| $\mathbf{q}$ | vector of generalized displacement |
| $a_1, b_1, c_1, d_1, a_2, b_2, c_2, d_2$ | parameters determining the geometry of gears 1 and 2 |
| $c_{xx}, c_{xy}, c_{yx}, c_{yy}$ | damping coefficients of journal bearing |
| $J_i^d, J_i^z$ | diametrical and polar moments of inertia of the $i$th mass |
| $k_1, k_2$ | torsional stiffness coefficients of the equivalent shaft in Figure 7 |
| $k_{xx}, k_{xy}, k_{yx}, k_{yy}$ | stiffness coefficients of journal bearing |
| $l_i$ | length of the $i$th shaft section |
| $m_i$ | lumped mass of the $i$th element |
| $n$ | total node number of two rotors |
| $r_{b1}, r_{b2}$ | base circle radii of bevel gears 1 and 2 |
| $r_{e1}, r_{e2}$ | base circle radii of the first and second virtual cylindrical gears |
| $x, y, z$ | Cartesian co-ordinates |
| $x_i, y_i, z_i$ | translational displacements of the mass center of the $i$th lumped mass |
| $\varphi_i, \psi_i, \theta_i$ | two tilting angles and torsional angle of the $i$th lumped mass |
| $\Theta_i, \Theta_2$ | rotational angles of gears 1 and 2 |
| $\Omega_1, \Omega_2$ | rotating speeds of rotors 1 and 2 |
| $\alpha$ | pressure angle of gear |
| $\delta_1, \delta_2$ | pitch cone angles of gears 1 and 2 |
| $\omega_{t1}, \omega_{t2}$ | the first and the second natural frequencies of torsional vibration in Figure 7 |
| $\omega$ | vector of angular velocity |

*Subscripts*

| | |
|---|---|
| $a, l, t$ | axial, lateral and torsional directions |
| $e$ | virtual cylindrical gear |
| 1, 2 | gears (or rotors) 1 and 2 |
| $i, j$ | the $i$th and $j$th shaft sections (or nodes) |
| $x, y$ | $x$ and $y$ components in lateral direction |

*Superscripts*

| | |
|---|---|
| $d, z$ | diameter and the $z$ (or polar) direction |
| ", " | the first and second order derivatives with respect to time |